

Orbital-Zeeman cross correlation in p - and d -wave altermagnets

Tomonari Mizoguchi¹ and Soshun Ozaki²

¹*Department of Physics, University of Tsukuba, 1-1-1 Tennodai, Tsukuba, Ibaraki 305-8571, Japan**

²*Max Planck Institute for Solid State Research, Heisenbergstrasse 1, D-70569 Stuttgart, Germany*

(Dated: March 11, 2026)

Altermagnets are a novel class of magnets that exhibit a large spin splitting but the total magnetic moment is vanishing. This unconventional spin splitting gives rise to various characteristic phenomena, such as spin current generation. In this paper, we study the orbital-Zeeman (OZ) cross term in altermagnets. Specifically, we consider the Rashba metal and the surface Dirac cones of three-dimensional topological insulators (TIs) in the presence of the altermagnetic order parameters. For the Rashba metals, the p -wave order parameter exerts only a limited influence on the OZ term, whereas the d -wave one causes the sign change of it when the order parameter becomes sufficiently large. For the TI surface, the p -wave order parameter retains the step-function-type dependence of the OZ term as a function of the chemical potential (μ) associated with the jump at $\mu = 0$, observed in the TI surface without magnetism, but its magnitude is reduced. For the d -wave case, the magnitude of jump at $\mu = 0$ is preserved but the OZ term decreases as increasing $|\mu|$.

I. INTRODUCTION

Itinerant electron systems with magnetic order exhibit a variety of intriguing physical phenomena. Such systems host a delicate interplay between electronic band structures, exchange interactions, and spin-orbit coupling, giving rise to unconventional transport responses and magnetoelectric effects. Examples include the topological and anomalous Hall effects in skyrmion systems [1–4] and kagome magnets [5–7]. Magnetism is also known to enrich the topological electronic structures; antiferromagnetic topological insulators (TIs) [8] and magnetically doped TIs [9, 10] are prominent examples.

In recent years, a novel type of magnetic order, dubbed altermagnets [11–15], has attracted considerable attention. Altermagnets possess properties that are distinct from those of conventional ferromagnets and antiferromagnets. Specifically, altermagnets exhibit spin splitting even in the absence of spin-orbit coupling, despite having zero net magnetization. Such a situation typically realizes when the opposite-spin sublattices are connected by rotation but not by translation or inversion. Spin splitting in altermagnets has attracted growing interest for its potential in spintronic applications, notably spin current generation [11–13, 16, 17]. Their characteristic optical responses [18, 19], nonlinear responses [20–22], the Edelstein effect [23, 24], the peizomagnetic effect [25, 26], as well as their impacts on other phases of matter such as topological phases [27, 28] and superconductivity [29–34], have also been actively studied. In parallel with theoretical investigations of the characteristic phenomena of altermagnets, considerable efforts have been devoted to finding the candidate materials by *ab initio* calculations [35–39] and group-theoretical considerations [40, 41], and to experimental detection in those materials [42–46].

In addition to the transport phenomena and optical responses, the response to the static magnetic field also reflects characteristics of the Bloch electrons. In fact, the orbital magnetic susceptibility comprises several contributions, including interband processes, a part of which encodes the topology and quantum geometry of the Bloch bands [47–53]. Additionally, when spin degrees of freedom and orbital motion are coupled, the magnetic susceptibility acquires additional terms originating from this coupling, which are referred to as the orbital-Zeeman (OZ) cross term [54–63]. This cross term also reflects the topological and geometrical aspects of Bloch electrons. In altermagnets, the magnetic order parameters possess a characteristic momentum dependence, so it is important to clarify how it affects the OZ cross response.

In this paper, we study the OZ term of the magnetic susceptibility for the two-dimensional altermagnetic Rashba metal [Fig. 1(a)] and the surface Dirac cones of the three-dimensional TI coupled to the altermagnet [Fig. 1(b)] [64]. We first point out that the altermagnetic order parameter alone cannot induce the OZ term; rather, the finite non-relativistic effect is necessary. In this sense, the altermagnetic order plays only a secondary role for the OZ term. For the Rashba metals, we numerically calculate χ_{OZ} in the low-temperature regime, focusing on its chemical potential (μ) dependence. We find that it can modify the OZ term both qualitatively and

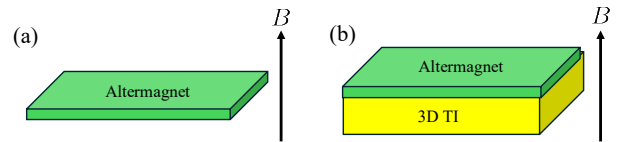


FIG. 1. Schematic figures of (a) the two-dimensional altermagnet and (b) the altermagnet placed on the three-dimensional TI.

* mizoguchi@rhodia.ph.tsukuba.ac.jp

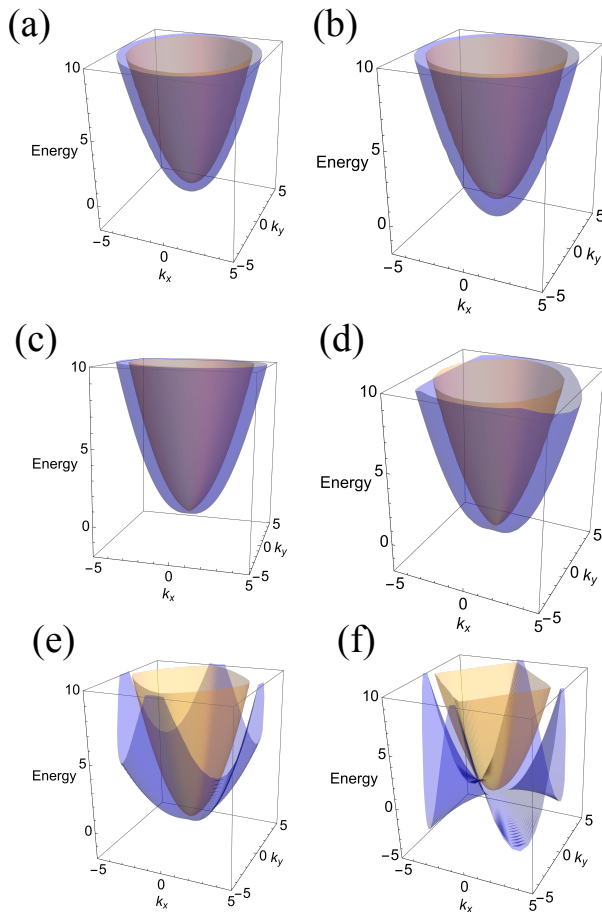


FIG. 2. Band structures for the s -wave case with (a) $J = 0.3$ and (b) $J = 0.6$, the p -wave case with (c) $J = 0.3$ and (d) $J = 0.6$, and the d -wave case with (e) $J = 0.3$ and (f) $J = 0.6$. We set $\frac{\hbar^2}{m} = 1$ and $\lambda = 0.3$.

quantitatively. To be specific, we find that the p -wave order parameter exerts a rather limited influence on the OZ term, whereas the d -wave one causes a sign change of it when the order parameter becomes sufficiently large. For the TI surface, we obtain the analytical expressions for χ_{OZ} at $T = 0$, and find that the p -wave order parameter retains the step-function-type dependence of the OZ term as a function of the chemical potential associated with the jump at $\mu = 0$, observed in the TI surface without magnetism, but its magnitude is reduced. For the d -wave case, the magnitude of jump at $\mu = 0$ is preserved but the OZ term decreases as increasing $|\mu|$. In addition, we also remark on the quantization of the jump with respect to the Berry curvature.

The rest of this paper is structured as follows. In Sec. II, we introduce the model. In Sec. III, we present the theoretical formulation to calculate χ_{OZ} . Our main results are presented in Sec. IV, where we show the numerical results on the Rashba metal, and the analytic result for the TI surface. Finally, we summarize this pa-

per in Sec. V.

In what follows, \hbar represents the reduced Planck constant, e (< 0) represents the electron charge, m represents the electron mass, μ_{B} represents the Bohr magneton, and k_{B} stands for the Boltzmann constant.

II. MODEL

We consider the Rashba metal and the surface Dirac cones of TIs in the presence of the altermagnetic order parameters with the out-of-plane Néel vector. The Hamiltonian in the momentum space reads

$$H_{\mathbf{k}} = h_{\mathbf{k}}^0 \sigma_0 + \mathbf{h}_{\mathbf{k}} \cdot \boldsymbol{\sigma}, \quad (1)$$

where $\mathbf{h}_{\mathbf{k}} = (h_{\mathbf{k}}^1, h_{\mathbf{k}}^2, h_{\mathbf{k}}^3)$ with $h_{\mathbf{k}}^1 = -\lambda k_y$, $h_{\mathbf{k}}^2 = \lambda k_x$, and $h_{\mathbf{k}}^3 = JX_{\mathbf{k}}^\ell$. Here, σ_0 stands for the 2×2 identity matrix and $\boldsymbol{\sigma} = (\sigma_x, \sigma_y, \sigma_z)$ are the Pauli matrices that represent the spin degrees of freedom. $X_{\mathbf{k}}^\ell$ describes the symmetry of the altermagnet with the ℓ -wave:

$$X_{\mathbf{k}}^\ell = \begin{cases} 1 & \ell = s, \\ k_x & \ell = p, \\ 2k_x k_y & \ell = d. \end{cases} \quad (2)$$

J (≥ 0) is the strength of the (alter)magnetic order parameter. Note that the s -wave corresponds to the conventional ferromagnet, which we consider for the purpose of comparison with the altermagnet. As for $h_{\mathbf{k}}^0$, when considering the Rashba metal, we set $h_{\mathbf{k}}^0 = \frac{\hbar^2 k^2}{2m}$ ($k = \sqrt{k_x^2 + k_y^2}$). In that case, λ stands for the coupling constant of the Rashba spin-orbit coupling. For the TI surface, we set $h_{\mathbf{k}}^0 = 0$, and in that case λ corresponds to $\lambda = \hbar v_{\text{F}}$ where v_{F} is the Fermi velocity of the Dirac cone.

In what follows, the band structure plays an important role in discussing χ_{OZ} of Rashba metals. In Fig. 2, we plot the band structures for the s -, p -, and d -wave cases. We see two key features. First, the upper and the lower bands are gapped for the s -wave case, whereas the gap closes at $\mathbf{k} = \mathbf{0}$ for p - and d -wave cases, which is attributed to the nodal structure of the order parameters. Second, only in the d -wave case, the lower band has no lower bound when J is sufficiently large. Specifically, we find that a band structure unbounded from below is realized when $J > \frac{\hbar^2}{2m}$.

III. ORBITAL-ZEEMAN CROSS CORRELATION

We calculate the magnetic susceptibility for the cross correlation between the orbital and Zeeman effects, χ_{OZ} , whose microscopic derivation has been given in Refs. [56, 58, 60, 63]. We consider the case where the magnetic field is in the z -direction, which is perpendicular to the

two-dimensional plane and is parallel to the Néel vector. In this case, χ_{OZ} is given as

$$\chi_{\text{OZ}} = \frac{i|e|\mu_{\text{B}}k_{\text{B}}T}{\hbar V} \sum_{n,\mathbf{k}} \text{Tr} [\sigma^3 \mathcal{G} \gamma_x \mathcal{G} \gamma_y \mathcal{G} - (x \leftrightarrow y)], \quad (3)$$

where

$$\mathcal{G} = (i\omega_n + \mu - H_{\mathbf{k}})^{-1} = \frac{1}{(i\omega_n - \xi_{\mathbf{k},+})(i\omega_n - \xi_{\mathbf{k},-})} \times \begin{pmatrix} i\omega_n + \mu - h_{\mathbf{k}}^0 + h_{\mathbf{k}}^3 & h_{\mathbf{k}}^1 - ih_{\mathbf{k}}^2 \\ h_{\mathbf{k}}^1 + ih_{\mathbf{k}}^2 & i\omega_n + \mu - h_{\mathbf{k}}^0 - h_{\mathbf{k}}^3 \end{pmatrix} \quad (4)$$

is the Matsubara Green's function with $\omega_n = (2n + 1)\pi k_{\text{B}}T$, $\gamma_\nu = \partial_{k_\nu} H_{\mathbf{k}}$ is the velocity operator in ν -direction multiplied by \hbar , and V is the area of the two dimensional system. In Eq. (4), we have used $\xi_{\mathbf{k},\pm} = h_{\mathbf{k}}^0 \pm h_{\mathbf{k}} - \mu$, with $h_{\mathbf{k}} := |\mathbf{h}_{\mathbf{k}}|$. For later use, we further define $\Omega_{\mathbf{k}}(i\omega_n) := i\omega_n + \mu - h_{\mathbf{k}}^0 = i\omega_n - \xi_{\mathbf{k}}^0$, with $\xi_{\mathbf{k}}^0 := h_{\mathbf{k}}^0 - \mu$.

Taking the trace in Eq. (3), we have

$$\begin{aligned} & \text{Tr} [\sigma^3 \mathcal{G} \gamma_x \mathcal{G} \gamma_y \mathcal{G} - (x \leftrightarrow y)] \\ &= \frac{4i\lambda^2}{(i\omega_n - \xi_{\mathbf{k},+})^3 (i\omega_n - \xi_{\mathbf{k},-})^3} \sum_{j=0}^3 P_{\mathbf{k},j}^\ell \Omega_{\mathbf{k}}^j, \end{aligned} \quad (5)$$

where $P_{\mathbf{k},j}^\ell$'s are given as

$$P_{\mathbf{k},0}^\ell = Y \cdot -\frac{\hbar^2 k^2}{m} h_{\mathbf{k}}^2, \quad (6a)$$

$$P_{\mathbf{k},1}^\ell = -h_{\mathbf{k}}^2 \quad (6b)$$

$$P_{\mathbf{k},2}^\ell = Y \cdot \hbar^2 \frac{k^2}{m} \quad (6c)$$

and

$$P_{\mathbf{k},3}^\ell = 1, \quad (6d)$$

where $Y = 1(0)$ for the Rashba metal (the TI surface). Note that $P_{\mathbf{k},2}^\ell$ and $P_{\mathbf{k},3}^\ell$ do not depend on ℓ . In Eq. (5), we see $\chi_{\text{OZ}} = 0$ if $\lambda = 0$, which means that the altermagnet alone cannot induce the OZ cross response. In fact, the spin is the good quantum number for $\lambda = 0$, meaning that \mathcal{G} and γ_j are the diagonal matrices. Therefore, we have $\sigma^3 \mathcal{G} \gamma_x \mathcal{G} \gamma_y \mathcal{G} = \sigma^3 \mathcal{G} \gamma_y \mathcal{G} \gamma_x \mathcal{G}$ as all the matrices commute with each other, resulting in the vanishing of χ_{OZ} .

To proceed further, we need to perform the summation over the Matsubara frequency. After some algebras (see Appendix A), we have the following expression:

$$\begin{aligned} & \chi_{\text{OZ}} \\ &= \frac{-4\lambda^2 |e|\mu_{\text{B}}}{\hbar} \int \frac{d^2 k}{(2\pi)^2} \left[\sum_{\alpha=\pm} G_{\mathbf{k},\alpha}^{\ell,(0)} f(\xi_{\mathbf{k},\alpha}) + G_{\mathbf{k},\alpha}^{\ell,(1)} f'(\xi_{\mathbf{k},\alpha}) \right], \end{aligned} \quad (7)$$

where

$$G_{\mathbf{k},\alpha}^{\ell,(0)} = \alpha \left[\frac{3}{16h_{\mathbf{k}}^5} P_{\mathbf{k},0}^\ell - \frac{1}{16h_{\mathbf{k}}^3} P_{\mathbf{k},2}^\ell \right] = -\frac{Y\alpha}{4h_{\mathbf{k}}^3} \frac{\hbar^2 k^2}{m}, \quad (8a)$$

and

$$\begin{aligned} & G_{\mathbf{k},\alpha}^{\ell,(1)} \\ &= -\frac{3}{16h_{\mathbf{k}}^4} P_{\mathbf{k},0}^\ell - \alpha \frac{1}{16h_{\mathbf{k}}^3} P_{\mathbf{k},1}^\ell + \frac{1}{16h_{\mathbf{k}}^2} P_{\mathbf{k},2}^\ell + \alpha \frac{3}{16h_{\mathbf{k}}} P_{\mathbf{k},3}^\ell \\ &= \frac{\alpha}{4h_{\mathbf{k}}} + \frac{Y}{4h_{\mathbf{k}}^2} \frac{\hbar^2 k^2}{m}, \end{aligned} \quad (8b)$$

where $f(x) = \frac{1}{e^{x/k_{\text{B}}T} + 1}$ is the Fermi-Dirac distribution function and $f'(x)$ is its derivative. It is to be noted that the term proportional to f vanishes for the TI surface. Without the altermagnet, (i.e., $J = 0$), analytic results are obtained for several cases, which correspond to the results of the previous works [55, 56]. We summarize those results in Appendices B and C. Note also that, for the TI surface, we derive the explicit forms of χ_{OZ} at any temperature for the s - and p -wave cases, and at $T = 0$ for the d -wave case. These results are also presented in Appendix C.

IV. RESULTS

A. Rashba metal

For the Rashba metal, we perform the integration over \mathbf{k} numerically. We set $k_{\text{B}}T = 0.01$ and $\frac{\hbar^2}{m} = 1$. For the integration over \mathbf{k} , we employ the radial coordinate $\int \frac{d^2 k}{(2\pi)^2} \rightarrow \frac{1}{(2\pi)^2} \int_0^{k_c} k dk \int_0^{2\pi} d\theta$, where $(k_x, k_y) = (k \cos \theta, k \sin \theta)$ and k_c is the momentum cut-off. Here we set $k_c = 6\pi$, which is far away from the Fermi surface except for the case of the d -wave with large J .

Figure 3 shows the μ dependence of χ_{OZ} for the Rashba metal with $\lambda = 0.3$. For comparison, we also plot the case of $J = 0$, which exhibits the diamagnetic susceptibility around $\mu = 0$. For the s -wave, which opens the band gap at $\mathbf{k} = 0$, χ_{OZ} is suppressed when μ lies in that gap [i.e., the case where only one Fermi surface remains as shown in Figs. 2(a) and 2(b)], and it has minima at the edge of that gap. In the p -wave case, the diamagnetic susceptibility is monotonically suppressed as J increases, which indicates that the p -wave order parameter affects the OZ term only in a quantitative manner. In contrast to the p -wave, we see a prominent change for d -wave. Namely, for sufficiently large J [i.e., $J = 0.6$ in Fig. 3(c)], we see that χ_{OZ} becomes positive for $\mu \lesssim -0.069$. This paramagnetic χ_{OZ} may be attributed to the unbounded lower band [Fig. 2(f)]. It then turns negative, and the diamagnetic susceptibility at the minimum of χ_{OZ} is enhanced compared with the $J = 0$ case.

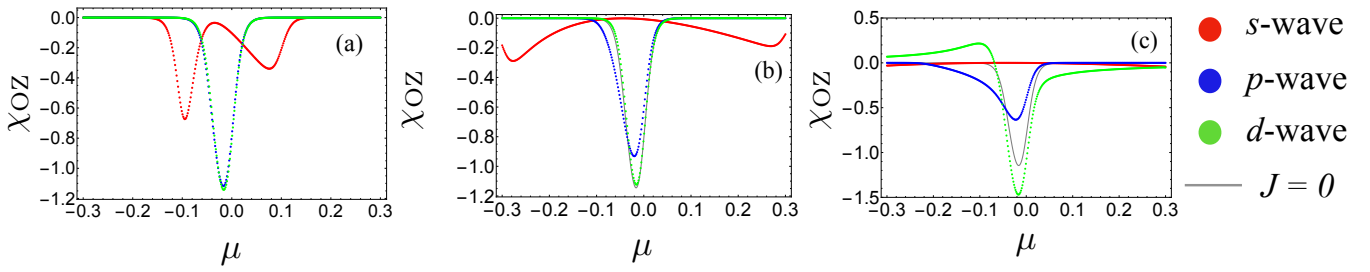


FIG. 3. μ dependence of χ_{OZ} for the Rashba metal for $\lambda = 0.3$ and (a) $J = 0.1$, (b) $J = 0.3$, and (c) $J = 0.6$. The unit of the vertical axis is $\frac{|e|\mu_B}{2\pi\hbar}$.

B. Topological insulator surface

As we have mentioned in the previous section, for the TI surface, we can perform the integration over \mathbf{k} analytically. The detailed derivation is given in Appendix C; here we summarize the results for $T = 0$. For the s -wave magnet, we have

$$\chi_{OZ} = \frac{|e|\mu_B}{2\pi\hbar} [\Theta(\mu - J) + \Theta(J + \mu) - 1], \quad (9)$$

for the p -wave magnet, we have

$$\chi_{OZ} = \text{sgn}(\mu) \frac{|e|\mu_B}{2\pi\hbar} \frac{\lambda}{\sqrt{\lambda^2 + J^2}}, \quad (10)$$

and for the d -wave magnet, we have

$$\chi_{OZ} = \text{sgn}(\mu) \frac{|e|\mu_B}{\hbar} \frac{K(w)}{\pi^2 \sqrt{1+w}}, \quad (11)$$

where $\Theta(x)$ represents the step function, $w = \frac{4J^2\mu^2}{\lambda^4}$, and $K(x)$ is the complete elliptic integral of the first kind. Note that for $J = 0$, i.e., the TI surface without magnetism, we have

$$\chi_{OZ} = \text{sgn}(\mu) \frac{|e|\mu_B}{2\pi\hbar}. \quad (12)$$

Note also that the results for the s -wave magnet as well as $J = 0$ as a limit of that were obtained by Ref. 55.

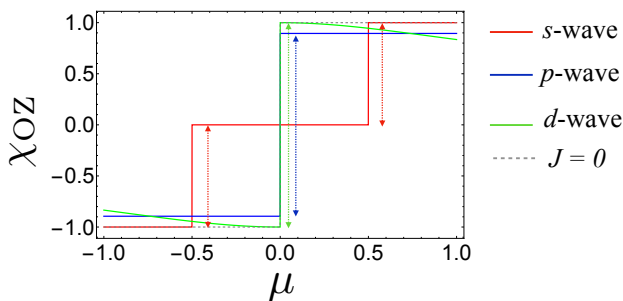


FIG. 4. μ dependence of χ_{OZ} for the TI surface with $\lambda = 1$ and $T = 0$. The unit of the vertical axis is $\frac{|e|\mu_B}{2\pi\hbar}$.

In Fig. 4, we plot the μ dependence of χ_{OZ} at $T = 0$ with $\lambda = 1$ and $J = 0.5$; for comparison, we also plot the case of $J = 0$. We see a jump of χ_{OZ} at $\mu = 0$ for $J = 0$, the p -wave, and the d -wave cases, and $\mu = \pm J$ for the s -wave case. As for the magnitude of the jump, we see that $\Delta\chi_{OZ} := \frac{|e|\mu_B}{\pi\hbar}$ for $J = 0$ and the d -wave case, which is the universal value, whereas $\Delta\chi_{OZ} := \frac{\lambda}{\sqrt{\lambda^2 + J^2}} \frac{|e|\mu_B}{\pi\hbar}$ for the p -wave, which is parameter dependent. For the s -wave, we see two jumps each of which has half of the magnitude of the $J = 0$ value.

In addition to the jump, we also find that, except for the d -wave case, χ_{OZ} exhibits the step-function μ dependence, namely, $\chi_{OZ} \propto \text{sgn}(\mu)$ for $J = 0$ and the p -wave, and $\chi_{OZ} \propto [\Theta(\mu - J) + \Theta(J + \mu) - 1]$ for the s -wave. For the d -wave, on the other hand, $|\chi_{OZ}|$ decreases as increasing $|\mu|$.

Finally, we address the origin of the quantized jump width in χ_{OZ} observed for the $J = 0$ and s -wave order parameters, both of which have particle-hole symmetry. Half of the contribution is interpreted as the orbital magnetization induced by the Zeeman field [54, 58, 60, 63]: For our two-band systems with particle-hole symmetry, the orbital magnetization at zero temperature is expressed as [65–69]

$$M_z(B) = \frac{|e|\mu}{\hbar} \sum_{\mathbf{k}, \pm} \Omega_z^\pm(\mathbf{k}) \Theta(\mu - E_{\mathbf{k}}^\pm(B)), \quad (13)$$

where $E_{\mathbf{k}}^\pm(B)$ and $\Omega_z^\pm(\mathbf{k})$ represent the energy dispersion of the conduction/valence band and its Berry curvature, respectively.

These expressions indicate that the Berry-curvature effect leads to the quantization of the jump, which is robust against spin-orbit coupling. We expect that the same mechanism is responsible for the d -wave order parameter case, which also possesses particle-hole symmetry.

V. SUMMARY

We have studied the orbital-Zeeman cross correlation of the altermagnets. We have considered the two cases, namely, the altermagnet in the presence of the Rashba spin-orbit coupling and the altermagnet coupled to the

surface Dirac cone of the three-dimensional TI. Although the effect of the altermagnetic order parameter is limited to be secondary, we find several characteristic features. For the Rashba metal, we find that the p -wave order parameter causes only quantitative changes in χ_{OZ} , whereas the d -wave can cause the qualitative change, such as the sign change, if the order parameter is large enough. For the TI surface, we obtain the analytical expressions for χ_{OZ} . To be precise, we obtain the full chemical potential and temperature dependence for the p -wave case, whereas for the d -wave case the analytic form is limited to the zero temperature. Focusing on the chemical potential dependence at the zero temperature, we find that the p -wave order parameter retains the step-function-type dependence of the OZ term as a function of the chemical potential associated with the jump at $\mu = 0$, observed in the TI surface without magnetism, but its magnitude becomes parameter dependent rather than the universal value. For the d -wave case, the jump at $\mu = 0$ is the universal value as is the case with $J = 0$, but the OZ term decreases as increasing $|\mu|$, which is dictated by the complete elliptic integral of the first kind. We have also elucidated that the quantization of the jump for the s -wave case originates from the Berry curvature effect.

ACKNOWLEDGMENTS

We thank Masao Ogata, Nobuyuki Okuma, and Ikuma Tateishi for fruitful discussions. This work is supported by JSPS KAKENHI, Grant No. JP23K03243 (TM).

Appendix A: Derivation of Eq. (7)

Here we describe the details of the summation over Matsubara frequency in Eq. (5). As is the standard method using the residue integral, we have

$$k_{\text{B}}T \sum_n \frac{\Omega^j}{(i\omega_n - \xi_{\mathbf{k},+})^3 (i\omega_n - \xi_{\mathbf{k},-})^3} = \frac{1}{2} [Q^j(\xi_+; \xi_-) + Q^j(\xi_-; \xi_+)], \quad (\text{A1})$$

where

$$Q^j(x; y) = \frac{d^2}{dx^2} \left[\frac{f(x)(\Omega_{\mathbf{k}}(x))^j}{(x-y)^3} \right]. \quad (\text{A2})$$

The explicit forms of $Q^j(x; y)$ are

$$Q^0(x; y) = \frac{f''(x)}{(x-y)^3} - \frac{6f'(x)}{(x-y)^4} + \frac{12f(x)}{(x-y)^5}, \quad (\text{A3a})$$

$$Q^1(x; y) = \frac{(x-\xi^0)}{(x-y)^3} f''(x) + \left[\frac{2}{(x-y)^3} - \frac{6(x-\xi^0)}{(x-y)^4} \right] f'(x) + \left[\frac{12(x-\xi^0)}{(x-y)^5} - \frac{6}{(x-y)^4} \right] f(x), \quad (\text{A3b})$$

$$Q^2(x; y) = \frac{(x-\xi^0)^2}{(x-y)^3} f''(x) + \left[\frac{4(x-\xi^0)}{(x-y)^3} - \frac{6(x-\xi^0)^2}{(x-y)^4} \right] f'(x) + \left[\frac{12(x-\xi^0)^2}{(x-y)^5} - \frac{12(x-\xi^0)}{(x-y)^4} + \frac{2}{(x-y)^3} \right] f(x), \quad (\text{A3c})$$

and

$$Q^3(x; y) = \frac{(x-\xi^0)^3}{(x-y)^3} f''(x) + \left[\frac{6(x-\xi^0)^2}{(x-y)^3} - \frac{6(x-\xi^0)^3}{(x-y)^4} \right] f'(x) + \left[\frac{12(x-\xi^0)^3}{(x-y)^5} - \frac{18(x-\xi^0)^2}{(x-y)^4} + \frac{6(x-\xi^0)}{(x-y)^3} \right] f(x). \quad (\text{A3d})$$

Using these, we have

$$k_{\text{B}}T \sum_n \frac{1}{(i\omega_n - \xi_{\mathbf{k},+})^3 (i\omega_n - \xi_{\mathbf{k},-})^3} = \frac{3[f(\xi_+) - f(\xi_-)]}{16h^5} - \frac{3[f'(\xi_+) + f'(\xi_-)]}{16h^4} + \frac{f''(\xi_+) - f''(\xi_-)}{16h^3}, \quad (\text{A4a})$$

$$k_{\text{B}}T \sum_n \frac{\Omega}{(i\omega_n - \xi_{\mathbf{k},+})^3 (i\omega_n - \xi_{\mathbf{k},-})^3} = -\frac{f'(\xi_+) - f'(\xi_-)}{16h^3} + \frac{f''(\xi_+) + f''(\xi_-)}{16h^2}, \quad (\text{A4b})$$

$$k_{\text{B}}T \sum_n \frac{\Omega^2}{(i\omega_n - \xi_{\mathbf{k},+})^3 (i\omega_n - \xi_{\mathbf{k},-})^3} = -\frac{[f(\xi_+) - f(\xi_-)]}{16h^3} + \frac{f'(\xi_+) + f'(\xi_-)}{16h^2} + \frac{f''(\xi_+) - f''(\xi_-)}{16h}, \quad (\text{A4c})$$

and

$$k_{\text{B}}T \sum_n \frac{\Omega^3}{(i\omega_n - \xi_{\mathbf{k},+})^3 (i\omega_n - \xi_{\mathbf{k},-})^3} = \frac{3[f'(\xi_+) - f'(\xi_-)]}{16h} + \frac{f''(\xi_+) + f''(\xi_-)}{16}. \quad (\text{A4d})$$

Here, we use the shorthand h to denote $\hbar k$. Substituting these into Eq. (5), we obtain the form of Eq. (7). Notice that the term proportional to f'' vanishes for both the Rashba metal and the TI surface.

Appendix B: Analytic results for Rashba metal

In this appendix, we show the analytic result on the Rashba metal without the altermagnetic order parameter, which was obtained by Ref. 56. In this case, we have

$$G_{\alpha}^{(0)} = -\frac{\alpha \hbar^2}{4m\lambda^3 k}, \quad (\text{B1})$$

and

$$G_{\alpha}^{(1)} = \frac{\hbar^2}{4m\lambda^2} + \frac{\alpha}{4\lambda k}. \quad (\text{B2})$$

Thus, we have

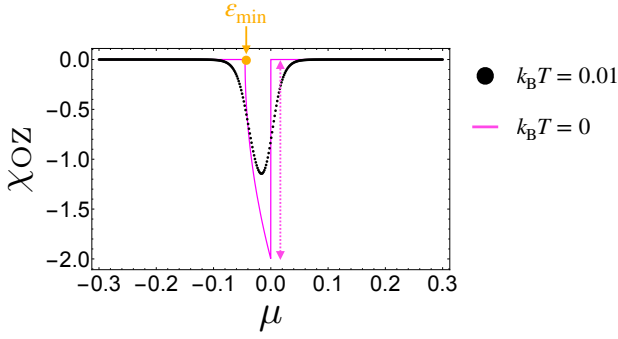


FIG. 5. μ dependence of χ_{OZ} for the Rashba metal with $\lambda = 0.3$. The black dots represent the numerical result with $k_{\text{B}}T = 0.01$ and the magenta line represent the result for $k_{\text{B}}T = 0$ [Eq. (B13)]. The unit of the vertical axis is $\frac{|e|\mu_{\text{B}}}{2\pi\hbar}$.

$$\chi_{\text{OZ}} = -\frac{\lambda^2|e|\mu_{\text{B}}}{2\pi\hbar} \sum_{\alpha=\pm} \int_0^{\infty} dk \left[-\frac{\alpha\hbar^2}{m\lambda^3} f(\xi_{\alpha}) + \left(\frac{\alpha}{\lambda} + \frac{\hbar^2 k}{m\lambda^2} \right) f'(\xi_{\alpha}) \right] = -\frac{\lambda^2|e|\mu_{\text{B}}}{2\pi\hbar} \sum_{\alpha=\pm} \int_0^{\infty} dk \left[-\frac{\alpha\hbar^2}{m\lambda^3} f(\xi_{\alpha}) + \frac{1}{\lambda^2} \frac{df(\xi_{\alpha})}{dk} \right]. \quad (\text{B3})$$

Note that we have used

$$\frac{d\xi_{\alpha}}{dk} = \frac{\hbar^2 k}{m} + \alpha\lambda = \lambda^2 \left(\frac{\alpha}{\lambda} + \frac{\hbar^2 k}{m\lambda^2} \right). \quad (\text{B4})$$

To proceed further, we consider the case of $T = 0$. We first consider the case of $\mu > 0$. In this case, we have

$$\int_0^{\infty} dk f(\xi_{\alpha}) = k_{\text{F},\alpha}, \quad (\text{B5})$$

where $k_{\text{F},\alpha}$ satisfies $\xi_{k_{\text{F},\alpha},\alpha} = 0$. To be specific, they are given as

$$k_{\text{F},\alpha} = \frac{m}{\hbar^2} \left(-\alpha\lambda + \sqrt{\lambda^2 + 2\mu\frac{\hbar^2}{m}} \right). \quad (\text{B6})$$

We also have

$$\int_0^{\infty} dk \frac{df(\xi_{\alpha})}{dk} = [\Theta(-\xi_{k,\alpha})]_0^{\infty} = -1. \quad (\text{B7})$$

Substituting these, we have

$$\begin{aligned} \chi_{\text{OZ}}(T=0, \mu > 0) &= -\frac{\lambda^2|e|\mu_{\text{B}}}{2\pi\hbar} \left[\frac{\hbar^2}{m\lambda^3} (k_{\text{F},-} - k_{\text{F},+}) - \frac{2}{\lambda^2} \right] \\ &= 0. \end{aligned} \quad (\text{B8})$$

Note that we have used $k_{\text{F},-} - k_{\text{F},+} = \frac{2m\lambda}{\hbar^2}$.

For $\mu < 0$, only the band $\alpha = -$ gives the finite contribution. In this case, we have

$$\int_0^{\infty} dk f(\xi_{-}) = \left(k_{\text{F},-}^{(1)} - k_{\text{F},-}^{(2)} \right) \Theta(\mu - \varepsilon_{\text{min}}), \quad (\text{B9})$$

where $\varepsilon_{\text{min}} = -\frac{\lambda^2 m}{2\hbar^2}$ is the bottom of the lower band, and

$$\begin{aligned} k_{\text{F},-}^{(1)} &= \frac{m}{\hbar^2} \left(\lambda + \sqrt{\lambda^2 + 2\mu\frac{\hbar^2}{m}} \right), \\ k_{\text{F},-}^{(2)} &= \frac{m}{\hbar^2} \left(\lambda - \sqrt{\lambda^2 + 2\mu\frac{\hbar^2}{m}} \right). \end{aligned} \quad (\text{B10})$$

We also have

$$\int_0^{\infty} dk \frac{df(\xi_{-})}{dk} = [\Theta(-\xi_{k,-})]_0^{\infty} = 0. \quad (\text{B11})$$

Then, we have

$$\chi_{\text{OZ}}(T=0, \mu < 0) = -\Theta(\mu - \varepsilon_{\text{min}}) \frac{|e|\mu_{\text{B}}}{2\pi\hbar} \left[\frac{2\sqrt{\lambda^2 + 2\mu\frac{\hbar^2}{m}}}{\lambda} \right]. \quad (\text{B12})$$

Combining these, we have

$$\chi_{\text{OZ}}(T=0) = -\frac{|e|\mu_{\text{B}}}{2\pi\hbar} \left[\frac{2\sqrt{\lambda^2 + 2\mu\frac{\hbar^2}{m}}}{\lambda} \right] \Theta(-\mu) \Theta(\mu - \varepsilon_{\text{min}}). \quad (\text{B13})$$

Note that χ_{OZ} exhibits a jump at $\mu = 0$, where χ_{OZ} is minimized, of magnitude $\frac{|e|\mu_{\text{B}}}{\pi\hbar}$, which is independent of the parameters.

In Fig. 5, we plot χ_{OZ} of Eq. (B13) for $\lambda = 0.3$, together with the numerical result for $k_{\text{B}}T = 0.01$. Comparing these two cases, we see that the minimum of χ_{OZ} is shifted to the finite $\mu (< 0)$ and the value of the minimum is largely reduced for $k_{\text{B}}T = 0.01$.

Appendix C: Analytic results for topological insulator surface

In this appendix, we show the derivations of Eqs. (9)-(12), that are, the analytic results on the TI surface. Note again that the results for $J = 0$ and the s -wave magnet are consistent with Ref. 55.

1. $J = 0$

For the TI surface without magnetism (i.e., $J = 0$), we have $\xi_{\pm} = \pm\lambda k - \mu$, $h = \lambda k$, $P_1 = -\lambda^2 k^2$, $P_3 = 1$, and $P_0 = P_2 = 0$, which leads to

$$G_{\alpha}^{(0)} = 0, \quad (\text{C1})$$

and

$$G_{\alpha}^{(1)} = \frac{\alpha}{4\lambda k}. \quad (\text{C2})$$

Therefore, we have

$$\begin{aligned} \chi_{\text{OZ}} &= -\frac{4\lambda^2|e|\mu_{\text{B}}}{\hbar} \int \frac{d^2k}{(2\pi)^2} \left[\sum_{\alpha=\pm} \frac{\alpha}{4\lambda k} f'(\alpha\lambda k - \mu) \right] \\ &= \frac{|e|\mu_{\text{B}}}{2\pi\hbar} [2f(-\mu) - 1]. \end{aligned} \quad (\text{C3})$$

For $T \rightarrow 0$, we have $f(-\mu) \rightarrow \frac{1+\text{sgn}(\mu)}{2}$ (if $|\mu| \neq 0$), thus $\chi_{\text{OZ}} \rightarrow \text{sgn}(\mu) \frac{|e|\mu_{\text{B}}}{2\pi\hbar}$.

2. s -wave magnet

For the s -wave magnet (i.e., the ordinary ferromagnet), where $X = 1$, we have $h = \sqrt{\lambda^2 k^2 + J^2}$ and $\xi_{\pm} = \pm\sqrt{\lambda^2 k^2 + J^2} - \mu$. We then have

$$\begin{aligned} \chi_{\text{OZ}} &= -\frac{4\lambda^2|e|\mu_{\text{B}}}{\hbar} \\ &\times \int \frac{d^2k}{(2\pi)^2} \left[\sum_{\alpha=\pm} \frac{\alpha}{4\sqrt{\lambda^2 k^2 + J^2}} f'(\alpha\sqrt{\lambda^2 k^2 + J^2} - \mu) \right] \\ &= \frac{|e|\mu_{\text{B}}}{2\pi\hbar} [f(J - \mu) + f(-J - \mu) - 1]. \end{aligned} \quad (\text{C4})$$

For $T \rightarrow 0$, we have $\chi_{\text{OZ}} \rightarrow \frac{|e|\mu_{\text{B}}}{2\pi\hbar} [\Theta(\mu - J) + \Theta(J + \mu) - 1]$.

3. p -wave magnet

For the p -wave magnet, where $X = k \cos \theta$, we have $h_{\mathbf{k}} = k\sqrt{\lambda^2 + J^2 \cos^2 \theta}$ and $\xi_{\pm} = \pm k\sqrt{\lambda^2 + J^2 \cos^2 \theta} - \mu$.

We then have

$$\begin{aligned} \chi_{\text{OZ}} &= -\frac{4\lambda^2|e|\mu_{\text{B}}}{\hbar} \int \frac{d^2k}{(2\pi)^2} \left[\sum_{\alpha=\pm} \frac{\alpha}{4h_{\mathbf{k}}} f'(\alpha h_{\mathbf{k}} - \mu) \right] \\ &= -\frac{\lambda^2|e|\mu_{\text{B}}}{(2\pi)^2\hbar} \int_0^{2\pi} d\theta \left\{ \frac{1}{\lambda^2 + J^2 \cos^2 \theta} \right. \\ &\quad \left. \int_0^{\infty} dk \left[\left(\frac{\partial f(h_{\mathbf{k}} - \mu)}{\partial k} \right) + \left(\frac{\partial f(-h_{\mathbf{k}} - \mu)}{\partial k} \right) \right] \right\} \\ &= \frac{|e|\mu_{\text{B}}}{2\pi\hbar} \frac{\lambda}{\sqrt{\lambda^2 + J^2}} [2f(-\mu) - 1]. \end{aligned} \quad (\text{C5})$$

Note that we have used

$$\begin{aligned} \left(\frac{\partial f(\alpha h_{\mathbf{k}} - \mu)}{\partial k} \right) &= \alpha \frac{\partial h_{\mathbf{k}}}{\partial k} f'(\alpha h_{\mathbf{k}} - \mu) \\ &= \alpha \sqrt{\lambda^2 + J^2 \cos^2 \theta} f'(\alpha h_{\mathbf{k}} - \mu), \end{aligned} \quad (\text{C6})$$

and

$$\int_0^{2\pi} \frac{d\theta}{\lambda^2 + J^2 \cos^2 \theta} = \frac{2\pi}{\lambda\sqrt{\lambda^2 + J^2}}. \quad (\text{C7})$$

For $T \rightarrow 0$, we have $\chi_{\text{OZ}} \rightarrow \text{sgn}(\mu) \frac{|e|\mu_{\text{B}}}{2\pi\hbar} \frac{\lambda}{\sqrt{\lambda^2 + J^2}}$.

4. d -wave magnet

For the d -wave magnet, where $X = k^2 \sin 2\theta$, we have $h_{\mathbf{k}} = \sqrt{\lambda^2 k^2 + J^2 k^4 \sin^2 2\theta}$ and $\xi_{\pm} = \pm\sqrt{\lambda^2 k^2 + J^2 k^4 \sin^2 2\theta} - \mu$. In this case, the analytical expression is obtained only when $T = 0$, so we focus on this case. Before proceeding further, we introduce the Fermi wave number that satisfies $h_{\mathbf{k}} = |\mu|$,

$$k_{\text{F}}(\theta) = \sqrt{\frac{\sqrt{\lambda^4 + 4\mu^2(J^2 \sin^2 2\theta)} - \lambda^2}{2(J^2 \sin^2 2\theta)}}. \quad (\text{C8})$$

Note that $k_{\text{F}}(\theta) \rightarrow \frac{|\mu|}{\lambda}$ for $\sin 2\theta \rightarrow 0$.

Turning to χ_{OZ} at $T = 0$, we have

$$\begin{aligned} \chi_{\text{OZ}} &= -\frac{4\lambda^2|e|\mu_{\text{B}}}{\hbar} \int \frac{d^2k}{(2\pi)^2} \left[\sum_{\alpha=\pm} \frac{\alpha}{4h_{\mathbf{k}}} f'(\alpha h_{\mathbf{k}} - \mu) \right] \\ &= \text{sgn}(\mu) \frac{\lambda^2|e|\mu_{\text{B}}}{(2\pi)^2\hbar} \int_0^{2\pi} d\theta \int_0^{\infty} dk \frac{k}{h_{\mathbf{k}}} \delta(h_{\mathbf{k}} - |\mu|) \\ &= \text{sgn}(\mu) \frac{\lambda^2|e|\mu_{\text{B}}}{(2\pi)^2\hbar} \int_0^{2\pi} d\theta \left[\frac{k}{h_{\mathbf{k}}} \left(\frac{\partial h_{\mathbf{k}}}{\partial k} \right)^{-1} \right]_{k=k_{\text{F}}(\theta)} \\ &= \text{sgn}(\mu) \frac{\lambda^2|e|\mu_{\text{B}}}{(2\pi)^2\hbar} \int_0^{2\pi} d\theta \frac{1}{\sqrt{1 + 4\frac{J^2\mu^2}{\lambda^4} \sin^2 2\theta}} \\ &= \frac{|e|\mu_{\text{B}}}{\hbar} \text{sgn}(\mu) \frac{K(w)}{\pi^2 \sqrt{1+w}}, \end{aligned} \quad (\text{C9})$$

where w and $K(x)$ are given as defined in the main text. Note that the jump at $\mu = 0$ is the same value as that of $J = 0$, since $K(0) = \frac{\pi}{2}$.

Appendix D: Detailed calculations of χ_{OZ} using the orbital magnetization

In this section, we present the detailed calculation of χ_{OZ} using the orbital magnetization. First, we consider s -wave order parameter case. Next, we discuss $J = 0$ case by taking $J \rightarrow 0$ limit.

1. Basic properties of Hamiltonian

The Hamiltonian in the momentum space under a Zeeman field reads

$$H_{\mathbf{k}} = \begin{pmatrix} \Delta & \lambda(-k_y - ik_x) \\ \lambda(-k_y + ik_x) & -\Delta \end{pmatrix}, \quad (\text{D1})$$

with $\Delta = J + \mu_B B$ ($\Delta > 0$). This Hamiltonian has particle-hole symmetry:

$$CH_{\mathbf{k}}C^{-1} = -H_{-\mathbf{k}}, \quad (\text{D2})$$

with $C = \sigma_x K$, where K is the complex conjugation operator. The wave functions for the valence and conduction bands are given as

$$|\psi_{\mathbf{k}}^-\rangle = \begin{pmatrix} \frac{\eta_{\mathbf{k}}}{2} \\ -ie^{i\theta_{\mathbf{k}}} \frac{\eta_{\mathbf{k}}}{2} \end{pmatrix}, \quad \text{for } E_{\mathbf{k}}^- = -E_{\mathbf{k}} \quad (\text{D3})$$

and

$$|\psi_{\mathbf{k}}^+\rangle = \begin{pmatrix} -ie^{-i\theta_{\mathbf{k}}} \frac{\eta_{\mathbf{k}}}{2} \\ \frac{\eta_{\mathbf{k}}}{2} \end{pmatrix}, \quad \text{for } E_{\mathbf{k}}^+ = E_{\mathbf{k}}, \quad (\text{D4})$$

where $E_{\mathbf{k}} = \sqrt{\lambda^2 k^2 + \Delta^2}$, $\tan \eta_{\mathbf{k}} = \frac{\lambda k}{\Delta}$ ($0 \leq \eta_{\mathbf{k}} < \frac{\pi}{2}$), and $\theta_{\mathbf{k}}$ is the polar angle corresponding to (k_x, k_y) ($0 \leq \theta_{\mathbf{k}} < 2\pi$). We confirm $C|\psi_{\mathbf{k}}^+\rangle = |\psi_{-\mathbf{k}}^-\rangle$ and $C|\psi_{\mathbf{k}}^-\rangle = |\psi_{-\mathbf{k}}^+\rangle$. The Berry curvatures for the valence and conduction bands are

$$\Omega_z^{\pm}(\mathbf{k}) = i \left(\left\langle \frac{\partial \psi_{\mathbf{k}}^{\pm}}{\partial k_x} \middle| \frac{\partial \psi_{\mathbf{k}}^{\pm}}{\partial k_y} \right\rangle - \text{c.c.} \right) = \mp \frac{1}{2} \frac{\lambda^2 \Delta}{E_{\mathbf{k}}^3}. \quad (\text{D5})$$

We note that the d -wave case is also particle-hole symmetric but p -wave case is not.

2. Calculation of χ_{OZ}

The integral of (13) is performed as follows.

$$M_z = \frac{|e|\mu V}{2\pi\hbar} \sum_{\pm} \int_0^{\infty} dk k \Omega_z^{\pm}(\mathbf{k}) \Theta(\mu - E_{\mathbf{k}}^{\pm}). \quad (\text{D6})$$

(i) $\mu < -|\Delta|$ case:

$$M_z = \frac{|e|\mu V}{2\pi\hbar} \int_{\sqrt{\mu^2 - \Delta^2}/\lambda}^{\infty} \frac{k \lambda^2 \Delta}{2(\lambda^2 k^2 + \Delta^2)^{3/2}} dk = -\frac{|e|\Delta V}{4\pi\hbar}. \quad (\text{D7})$$

Substituting $\Delta \rightarrow J + \mu_B B$ and expanding with respect to B , we obtain

$$\frac{1}{2} \chi_{\text{OZ}} = \frac{1}{V} \frac{\partial M_z}{\partial B} = -\frac{|e|\mu_B}{4\pi\hbar}. \quad (\text{D8})$$

(ii) $-|\Delta| < \mu < |\Delta|$ case:

$$M_z = \frac{|e|\mu V}{2\pi\hbar} \int_0^{\infty} \frac{k \cdot \lambda^2 \Delta}{2(\lambda^2 k^2 + \Delta^2)^{3/2}} dk = \frac{|e|\mu V}{4\pi\hbar}. \quad (\text{D9})$$

Therefore,

$$\frac{1}{2} \chi_{\text{OZ}} = \frac{1}{V} \frac{\partial M_z}{\partial B} = 0. \quad (\text{D10})$$

(iii) $|\Delta| < \mu$ case:

$$\begin{aligned} M_z &= \frac{|e|\mu V}{2\pi\hbar} \left(\frac{1}{2} + \int_0^{\sqrt{\mu^2 - \Delta^2}/\lambda} \frac{-k \cdot \lambda^2 \Delta}{2(\lambda^2 k^2 + \Delta^2)^{3/2}} dk \right) \\ &= \frac{|e|\Delta V}{4\pi\hbar}. \end{aligned} \quad (\text{D11})$$

Substituting $\Delta \rightarrow J + \mu_B B$ and expanding with respect to B , we obtain

$$\frac{1}{2} \chi_{\text{OZ}} = \frac{1}{V} \frac{\partial M_z}{\partial B} = \frac{|e|\mu_B}{4\pi\hbar}. \quad (\text{D12})$$

In summary, χ_{OZ} is given as

$$\chi_{\text{OZ}} = \frac{|e|\mu_B}{2\pi\hbar} \text{sgn}(\mu) \Theta(|\mu| - J), \quad (\text{D13})$$

which is exactly the same as the value obtained in the main text at $T = 0$. Finally, taking the $J \rightarrow 0$ limit, the $J = 0$ case is reproduced. These results show that the Berry curvature is responsible for the quantization of the jump observed in the $J = 0$ and s -wave order parameter cases.

[1] M. Lee, W. Kang, Y. Onose, Y. Tokura, and N. P. Ong, Unusual Hall Effect Anomaly in MnSi under Pressure,

Phys. Rev. Lett. **102**, 186601 (2009).

[2] A. Neubauer, C. Pfleiderer, B. Binz, A. Rosch, R. Ritz,

- P. G. Niklowitz, and P. Böni, Topological Hall Effect in the A Phase of MnSi, *Phys. Rev. Lett.* **102**, 186602 (2009).
- [3] N. Nagaosa and Y. Tokura, Topological properties and dynamics of magnetic skyrmions, *Nature Nanotechnology* **8**, 899 (2013).
- [4] T. Kurumaji, T. Nakaajima, M. Hirschberger, A. Kikkawa, Y. Yamasaki, H. Sagayama, H. Nakao, Y. Taguchi, T. hisa Arima, and Y. Tokura, Skyrmion lattice with a giant topological Hall effect in a frustrated triangular-lattice magnet, *Science* **365**, 914 (2019).
- [5] S. Nakatsuji, N. Kiyohara, and T. Higo, Large anomalous Hall effect in a non-collinear antiferromagnet at room temperature, *Nature* **527**, 212 (2015).
- [6] M. Ikhlas, T. Tomita, T. Koretsune, M.-T. Suzuki, D. Nishio-Hamane, R. Arita, Y. Otani, and S. Nakatsuji, Large anomalous Nernst effect at room temperature in a chiral antiferromagnet, *Nature Physics* **13**, 1085 (2017).
- [7] S.-Y. Yang, Y. Wang, B. R. Ortiz, D. Liu, J. Gayles, E. Derunova, R. Gonzalez-Hernandez, L. Šmejkal, Y. Chen, S. S. P. Parkin, S. D. Wilson, E. S. Toberer, T. McQueen, and M. N. Ali, Giant, unconventional anomalous Hall effect in the metallic frustrated magnet candidate, KV_3Sb_5 , *Science Advances* **6**, eabb6003 (2020).
- [8] R. S. K. Mong, A. M. Essin, and J. E. Moore, Antiferromagnetic topological insulators, *Phys. Rev. B* **81**, 245209 (2010).
- [9] C.-Z. Chang, J. Zhang, X. Feng, J. Shen, Z. Zhang, M. Guo, K. Li, Y. Ou, P. Wei, L.-L. Wang, Z.-Q. Ji, Y. Feng, S. Ji, X. Chen, J. Jia, X. Dai, Z. Fang, S.-C. Zhang, K. He, Y. Wang, L. Lu, X.-C. Ma, and Q.-K. Xue, Experimental Observation of the Quantum Anomalous Hall Effect in a Magnetic Topological Insulator, *Science* **340**, 167 (2013).
- [10] R. Yoshimi, K. Yasuda, A. Tsukazaki, K. S. Takahashi, N. Nagaosa, M. Kawasaki, and Y. Tokura, Quantum Hall states stabilized in semi-magnetic bilayers of topological insulators, *Nat. Commun.* **6**, 8530 (2015).
- [11] M. Naka, S. Hayami, H. Kusunose, Y. Yanagi, Y. Motome, and H. Seo, Spin current generation in organic antiferromagnets, *Nat. Commun.* **10**, 4305 (2019).
- [12] L. Šmejkal, J. Sinova, and T. Jungwirth, Beyond Conventional Ferromagnetism and Antiferromagnetism: A Phase with Nonrelativistic Spin and Crystal Rotation Symmetry, *Phys. Rev. X* **12**, 031042 (2022).
- [13] L. Šmejkal, J. Sinova, and T. Jungwirth, Emerging Research Landscape of Altermagnetism, *Phys. Rev. X* **12**, 040501 (2022).
- [14] A. B. Hellenes, T. Jungwirth, R. Jaeschke-Ubiergo, A. Chakraborty, J. Sinova, and L. Šmejkal, “P-wave magnets”, arXiv:2309.01607.
- [15] P. A. McClarty and J. G. Rau, Landau Theory of Altermagnetism, *Phys. Rev. Lett.* **132**, 176702 (2024).
- [16] M. Naka, Y. Motome, and H. Seo, Perovskite as a spin current generator, *Phys. Rev. B* **103**, 125114 (2021).
- [17] M. Naka, Y. Motome, and H. Seo, Altermagnetic perovskites, *npj Spintronics* **3**, 1 (2025).
- [18] M. Ezawa, Bulk photovoltaic effects in altermagnets, *Phys. Rev. B* **111**, L201405 (2025).
- [19] M. Ezawa, Quantum geometry and elliptic optical dichroism in p -wave magnets, *Phys. Rev. B* **112**, 045302 (2025).
- [20] Y. Fang, J. Cano, and S. A. A. Ghorashi, Quantum Geometry Induced Nonlinear Transport in Altermagnets, *Phys. Rev. Lett.* **133**, 106701 (2024).
- [21] M. Ezawa, Intrinsic nonlinear conductivity induced by quantum geometry in altermagnets and measurement of the in-plane Néel vector, *Phys. Rev. B* **110**, L241405 (2024).
- [22] M. Ezawa, Third-order and fifth-order nonlinear spin-current generation in g -wave and i -wave altermagnets and perfectly nonreciprocal spin current in f -wave magnets, *Phys. Rev. B* **111**, 125420 (2025).
- [23] M. Ezawa, Out-of-plane Edelstein effects: Electric field induced magnetization in p -wave magnets, *Phys. Rev. B* **111**, L161301 (2025).
- [24] A. Chakraborty, A. Birk Hellenes, R. Jaeschke-Ubiergo, T. Jungwirth, L. Šmejkal, and J. Sinova, Highly efficient non-relativistic Edelstein effect in nodal p -wave magnets, *Nat. Commun.* **16**, 7270 (2025).
- [25] M. Naka, Y. Motome, T. Miyazaki, and H. Seo, Nonrelativistic Piezomagnetic Effect in an Organic Altermagnet, *J. Phys. Soc. Jpn.* **94**, 083702 (2025).
- [26] Y. Ogawa and S. Hayami, Nonlinear Piezomagnetic Effects in g -wave Altermagnets, *J. Phys. Soc. Jpn.* **94**, 063704 (2025).
- [27] M. Ezawa, Detecting the Néel vector of altermagnets in heterostructures with a topological insulator and a crystalline valley-edge insulator, *Phys. Rev. B* **109**, 245306 (2024).
- [28] M. Ezawa, Topological insulators and superconductors based on p -wave magnets: Electrical control and detection of a domain wall, *Phys. Rev. B* **110**, 165429 (2024).
- [29] S. Sumita, M. Naka, and H. Seo, Fulde-Ferrell-Larkin-Ovchinnikov state induced by antiferromagnetic order in κ -type organic conductors, *Phys. Rev. Res.* **5**, 043171 (2023).
- [30] D. Chakraborty and A. M. Black-Schaffer, Zero-field finite-momentum and field-induced superconductivity in altermagnets, *Phys. Rev. B* **110**, L060508 (2024).
- [31] P. Sukhachov, H. G. Giil, B. Brekke, and J. Linder, Coexistence of p -wave magnetism and superconductivity, *Phys. Rev. B* **111**, L220403 (2025).
- [32] K. Mukasa and Y. Masaki, Finite-momentum Superconductivity in Two-dimensional Altermagnets with a Rashba-type Spin–Orbit Coupling, *J. Phys. Soc. Jpn.* **94**, 064705 (2025).
- [33] D. Chakraborty and A. M. Black-Schaffer, Perfect Superconducting Diode Effect in Altermagnets, *Phys. Rev. Lett.* **135**, 026001 (2025).
- [34] S. Sumita, M. Naka, and H. Seo, Phase-modulated superconductivity via altermagnetism, *Phys. Rev. B* **112**, 144510 (2025).
- [35] Y. Noda, K. Ohno, and S. Nakamura, Momentum-dependent band spin splitting in semiconducting MnO₂: a density functional calculation, *Phys. Chem. Chem. Phys.* **18**, 13294 (2016).
- [36] K.-H. Ahn, A. Hariki, K.-W. Lee, and J. Kuneš, Antiferromagnetism in RuO₂ as d -wave Pomeranchuk instability, *Phys. Rev. B* **99**, 184432 (2019).
- [37] L.-D. Yuan, Z. Wang, J.-W. Luo, E. I. Rashba, and A. Zunger, Giant momentum-dependent spin splitting in centrosymmetric low- Z antiferromagnets, *Phys. Rev. B* **102**, 014422 (2020).
- [38] I. I. Mazin, K. Koepernik, M. D. Johannes, R. González-Hernández, and L. Šmejkal, Prediction of unconventional magnetism in doped FeSb₂, *Proc. Nat. Acad. Sci.* **118**, e2108924118 (2021).

- [39] H.-Y. Ma, M. Hu, N. Li, J. Liu, W. Yao, J.-F. Jia, and J. Liu, Multifunctional antiferromagnetic materials with giant piezomagnetism and noncollinear spin current, *Nat. Commun.* **12**, 2846 (2021).
- [40] S. Hayami, Y. Yanagi, and H. Kusunose, Momentum-Dependent Spin Splitting by Collinear Antiferromagnetic Ordering, *J. Phys. Soc. Jpn.* **88**, 123702 (2019).
- [41] S. Hayami, Y. Yanagi, and H. Kusunose, Bottom-up design of spin-split and reshaped electronic band structures in antiferromagnets without spin-orbit coupling: Procedure on the basis of augmented multipoles, *Phys. Rev. B* **102**, 144441 (2020).
- [42] R. González-Hernández, L. Šmejkal, K. Výborný, Y. Yahagi, J. Sinova, T. c. v. Jungwirth, and J. Železný, Efficient Electrical Spin Splitter Based on Nonrelativistic Collinear Antiferromagnetism, *Phys. Rev. Lett.* **126**, 127701 (2021).
- [43] Z. Feng, X. Zhou, L. Šmejkal, L. Wu, Z. Zhu, H. Guo, R. González-Hernández, X. Wang, H. Yan, P. Qin, X. Zhang, H. Wu, H. Chen, Z. Meng, L. Liu, Z. Xia, J. Sinova, T. Jungwirth, and Z. Liu, An anomalous Hall effect in altermagnetic ruthenium dioxide, *Nature Electronics* **5**, 735 (2022).
- [44] R. D. Gonzalez Betancourt, J. Zubáč, R. Gonzalez-Hernandez, K. Geishendorf, Z. Šobáň, G. Springholz, K. Olejník, L. Šmejkal, J. Sinova, T. Jungwirth, S. T. B. Goennenwein, A. Thomas, H. Reichlová, J. Železný, and D. Krieger, Spontaneous Anomalous Hall Effect Arising from an Unconventional Compensated Magnetic Phase in a Semiconductor, *Phys. Rev. Lett.* **130**, 036702 (2023).
- [45] S. Iguchi, H. Kobayashi, Y. Ikemoto, T. Furukawa, H. Itoh, S. Iwai, T. Moriwaki, and T. Sasaki, Magneto-optical spectra of an organic antiferromagnet as a candidate for an altermagnet, *Phys. Rev. Res.* **7**, 033026 (2025).
- [46] R. Yamada, M. T. Birch, P. R. Baral, S. Okumura, R. Nakano, S. Gao, M. Ezawa, T. Nomoto, J. Masell, Y. Ishihara, K. K. Kolincio, I. Belopolski, H. Sagayama, H. Nakao, K. Ohishi, T. Ohhara, R. Kiyonagi, T. Nakajima, Y. Tokura, T.-h. Arima, Y. Motome, M. M. Hirschmann, and M. Hirschberger, A metallic p-wave magnet with commensurate spin helix, *Nature* **646**, 837 (2025).
- [47] H. Fukuyama and R. Kubo, Interband Effect on Magnetic Susceptibility. I. A Simple Two-Band Model, *J. Phys. Soc. Jpn.* **27**, 604 (1969).
- [48] H. Fukuyama, Theory of Orbital Magnetism of Bloch Electrons: Coulomb Interactions, *Prog. Theor. Phys.* **45**, 704 (1971).
- [49] M. Koshino and T. Ando, Diamagnetism in disordered graphene, *Phys. Rev. B* **75**, 235333 (2007).
- [50] G. Gómez-Santos and T. Stauber, Measurable Lattice Effects on the Charge and Magnetic Response in Graphene, *Phys. Rev. Lett.* **106**, 045504 (2011).
- [51] M. Ogata and H. Fukuyama, Orbital Magnetism of Bloch Electrons I. General Formula, *J. Phys. Soc. Jpn.* **84**, 124708 (2015).
- [52] Y. Gao, S. A. Yang, and Q. Niu, Geometrical effects in orbital magnetic susceptibility, *Phys. Rev. B* **91**, 214405 (2015).
- [53] F. Piéchon, A. Raoux, J.-N. Fuchs, and G. Montambaux, Geometric orbital susceptibility: Quantum metric without Berry curvature, *Phys. Rev. B* **94**, 134423 (2016).
- [54] S. Murakami, Quantum Spin Hall Effect and Enhanced Magnetic Response by Spin-Orbit Coupling, *Phys. Rev. Lett.* **97**, 236805 (2006).
- [55] Y. Tserkovnyak, D. A. Pesin, and D. Loss, Spin and orbital magnetic response on the surface of a topological insulator, *Phys. Rev. B* **91**, 041121 (2015).
- [56] H. Suzuura and T. Ando, Theory of magnetic response in two-dimensional giant Rashba system, *Phys. Rev. B* **94**, 085303 (2016).
- [57] M. Koshino and I. F. Hizbullah, Magnetic susceptibility in three-dimensional nodal semimetals, *Phys. Rev. B* **93**, 045201 (2016).
- [58] R. Nakai and K. Nomura, Crossed responses of spin and orbital magnetism in topological insulators, *Phys. Rev. B* **93**, 214434 (2016).
- [59] Y. Ominato, S. Tatsumi, and K. Nomura, Spin-orbit crossed susceptibility in topological Dirac semimetals, *Phys. Rev. B* **99**, 085205 (2019).
- [60] S. Ozaki and M. Ogata, Universal quantization of the magnetic susceptibility jump at a topological phase transition, *Phys. Rev. Res.* **3**, 013058 (2021).
- [61] Y. Araki, D. Suenaga, K. Suzuki, and S. Yasui, Spin-orbital magnetic response of relativistic fermions with band hybridization, *Phys. Rev. Res.* **3**, 023098 (2021).
- [62] A. Shitade and G. Tatara, Spin accumulation without spin current, *Phys. Rev. B* **105**, L201202 (2022).
- [63] S. Ozaki and M. Ogata, Topological contribution to magnetism in the Kane-Mele model: An explicit wavefunction approach, *Phys. Rev. B* **107**, 085201 (2023).
- [64] F. Qin and R. Chen, "Layer Hall effect induced by altermagnetism", arXiv:2601.03937.
- [65] D. Xiao, J. Shi, and Q. Niu, Berry Phase Correction to Electron Density of States in Solids, *Phys. Rev. Lett.* **95**, 137204 (2005).
- [66] T. Thonhauser, D. Ceresoli, D. Vanderbilt, and R. Resta, Orbital Magnetization in Periodic Insulators, *Phys. Rev. Lett.* **95**, 137205 (2005).
- [67] D. Xiao, W. Yao, and Q. Niu, Valley-Contrasting Physics in Graphene: Magnetic Moment and Topological Transport, *Phys. Rev. Lett.* **99**, 236809 (2007).
- [68] I. Souza and D. Vanderbilt, Dichroic f -sum rule and the orbital magnetization of crystals, *Phys. Rev. B* **77**, 054438 (2008).
- [69] M. Ogata, Theory of Magnetization in Bloch Electron Systems, *J. Phys. Soc. Jpn.* **86**, 044713 (2017).